



A radiomics approach to predict lymph node metastasis and clinical outcome of intrahepatic cholangiocarcinoma

Gu-Wei Ji^{1,2} · Fei-Peng Zhu³ · Yu-Dong Zhang³ · Xi-Sheng Liu³ · Fei-Yun Wu³ · Ke Wang^{1,2} · Yong-Xiang Xia^{1,2} · Yao-Dong Zhang^{1,2} · Wang-Jie Jiang^{1,2} · Xiang-Cheng Li^{1,2} · Xue-Hao Wang^{1,2}

Received: 15 November 2018 / Revised: 19 February 2019 / Accepted: 8 March 2019 / Published online: 26 March 2019
© European Society of Radiology 2019

Abstract

Objectives This study was conducted in order to establish and validate a radiomics model for predicting lymph node (LN) metastasis of intrahepatic cholangiocarcinoma (IHC) and to determine its prognostic value.

Methods For this retrospective study, a radiomics model was developed in a primary cohort of 103 IHC patients who underwent curative-intent resection and lymphadenectomy. Radiomics features were extracted from arterial phase computed tomography (CT) scans. A radiomics signature was built based on highly reproducible features using the least absolute shrinkage and selection operator (LASSO) method. Multivariate logistic regression analysis was adopted to establish a radiomics model incorporating radiomics signature and other independent predictors. Model performance was determined by its discrimination, calibration, and clinical usefulness. The model was internally validated in 52 consecutive patients.

Results The radiomics signature comprised eight LN-status-related features and showed significant association with LN metastasis in both cohorts ($p < 0.001$). A radiomics nomogram that incorporates radiomics signature and CA 19-9 level showed good calibration and discrimination in the primary cohort (AUC 0.8462) and validation cohort (AUC 0.8921). Promisingly, the radiomics nomogram yielded an AUC of 0.9224 in the CT-reported LN-negative subgroup. Decision curve analysis confirmed the clinical utility of this nomogram. High risk for metastasis portended significantly lower overall and recurrence-free survival than low risk for metastasis (both $p < 0.001$). The radiomics nomogram was an independent preoperative predictor of overall and recurrence-free survival.

Conclusions Our radiomics model provided a robust diagnostic tool for prediction of LN metastasis, especially in CT-reported LN-negative IHC patients, that may facilitate clinical decision-making.

Key Points

- The radiomics nomogram showed good performance for prediction of LN metastasis in IHC patients, particularly in the CT-reported LN-negative subgroup.
- Prognosis of high-risk patients remains dismal after curative-intent resection.
- The radiomics model may facilitate clinical decision-making and define patient subsets benefiting most from surgery.

Keywords Cholangiocarcinoma · Nomogram · Lymphatic metastasis · Decision support techniques · Radiomics

Gu-Wei Ji and Fei-Peng Zhu contributed equally to this work.

Electronic supplementary material The online version of this article (<https://doi.org/10.1007/s00330-019-06142-7>) contains supplementary material, which is available to authorized users.

✉ Xiang-Cheng Li
drxcli@njmu.edu.cn

✉ Xue-Hao Wang
wangxh@njmu.edu.cn

¹ Hepatobiliary Center, The First Affiliated Hospital of Nanjing Medical University, 300 Guangzhou Road, Nanjing 210029, People's Republic of China

² Key Laboratory of Liver Transplantation, Chinese Academy of Medical Sciences, Nanjing, People's Republic of China

³ Department of Radiology, The First Affiliated Hospital of Nanjing Medical University, Nanjing, People's Republic of China

Abbreviations

BTC	Biliary tract cancer
DCA	Decision curve analysis
IHC	Intrahepatic cholangiocarcinoma
ICC	Intraclass correlation coefficient
LASSO	Least absolute shrinkage and selection operator
NPV	Negative predictive value
OS	Overall survival
PPV	Positive predictive value
RFS	Recurrence-free survival
ROC	Receiver operating characteristic curve
ROI	Region of interest
VIF	Variance inflation factor

Introduction

Intrahepatic cholangiocarcinoma (IHC) is the second most common primary liver malignancy after hepatocellular carcinoma, and the global disease incidence is increasing [1]. According to macroscopic growth pattern, IHC can be categorized as mass-forming, periductal-infiltrating, or intraductal types, and mass-forming tumor is the most common type [2]. Radical resection offers the only chance for prolonged survival, with 5-year survival rate of 15–40% [3]. Unfortunately, fewer than 40% of IHC patients have early-stage disease that is amenable to surgery, and tumor recurrence occurs in up to 50–70% of patients after curative-intent resection [3, 4].

Lymph node (LN) metastasis is the most prominent malignant trait as well as the most relevant adverse prognostic factor following surgery for IHCs. Metastatic nodal disease has been reported in 20–60% of IHCs undergoing lymphadenectomy, and median survival after resection for IHCs with LN metastasis ranges from 6.6 to 24.0 months [5–7]. Despite this, the role of routine lymphadenectomy remains controversial, especially for IHCs without nodal swelling. Although removal of clinically apparent nodal disease is mandatory, some investigators have argued that nodal dissection does not provide therapeutic benefit [3, 8]. According to management guidelines, node-positive disease is a relative contraindication to surgery, and postoperative adjuvant therapy should be strongly considered for patients with nodal metastasis [3, 9]. Consequently, accurate staging of nodal status is a key step in IHC management.

Preoperative determination of nodal status is difficult based on conventional imaging procedures. Computed tomography (CT) has long been the standard imaging method for assessment of tumor extent but exhibits limited ability to detect nodal involvement, with a sensitivity of 30–50% [10, 11]. Recent advances in computer-assisted imaging techniques have facilitated the high-throughput extraction of quantitative features from digital medical images. This approach, termed radiomics, enables mineable high-dimensional data to be

applied within clinical decision support [12–14]. A set of imaging biomarkers provides a powerful tool for predicting LN metastasis in several solid tumors [15–17]. A recent study has demonstrated that radiomics features at portal phase CT can facilitate prediction of nodal metastasis in biliary tract cancers (BTCs) [18]. However, BTCs, which encompass intra- and extrahepatic cholangiocarcinoma and gallbladder carcinoma, are a diverse collection of tumors that may hinder the reproduction of results in a particular subset. Moreover, a relationship has been established between arterial enhancement and presence of LN metastasis: a relatively larger area of arterial enhancement of IHC is associated with a lower rate of LN metastasis [2, 19, 20]. To our knowledge, radiomics-based approach for predicting LN metastasis in IHCs has not yet been established.

Accordingly, the aim of this study was to develop and validate a radiomics model for preoperative prediction of LN metastasis in IHCs. Furthermore, we assessed the prognostic value of the radiomics model.

Materials and methods

Patients

The ethics committee of Nanjing Medical University approved this retrospective analysis and waived the requirement for informed consent. Patients who underwent curative-intent resection and lymphadenectomy for IHC between June 2010 and March 2018 were identified from the institutional database. [Supplementary methods](#) and [Fig. S1](#) present the inclusion and exclusion criteria as well as the patient recruitment pathway. A total of 155 patients were enrolled and divided into two independent cohorts: 103 patients treated between June 2010 and January 2016 constituted the primary cohort, while 52 patients treated from February 2016 to March 2018 constituted the validation cohort. Clinical data were obtained by reviewing the hospital records. The cutoff for carbohydrate antigen (CA) 19-9 level was 1000 U/ml because CA 19-9 concentration higher than 1000 U/ml is consistent with metastatic disease [1, 10].

CT image acquisition, tumor segmentation, and radiomics feature extraction

All patients were evaluated with contrast-enhanced CT and specific imaging parameters are detailed in the [Supplementary methods](#). Two radiologists (F.P.Z. and Y.D.Z. with 10 and 12 years of experience in abdominal imaging, respectively), blinded to the pathologic details and prognosis, reviewed transverse CT images in consensus to determine the following features: (a) tumor size, defined as maximum diameter on images; (b) tumor location, subclassified into perihilar

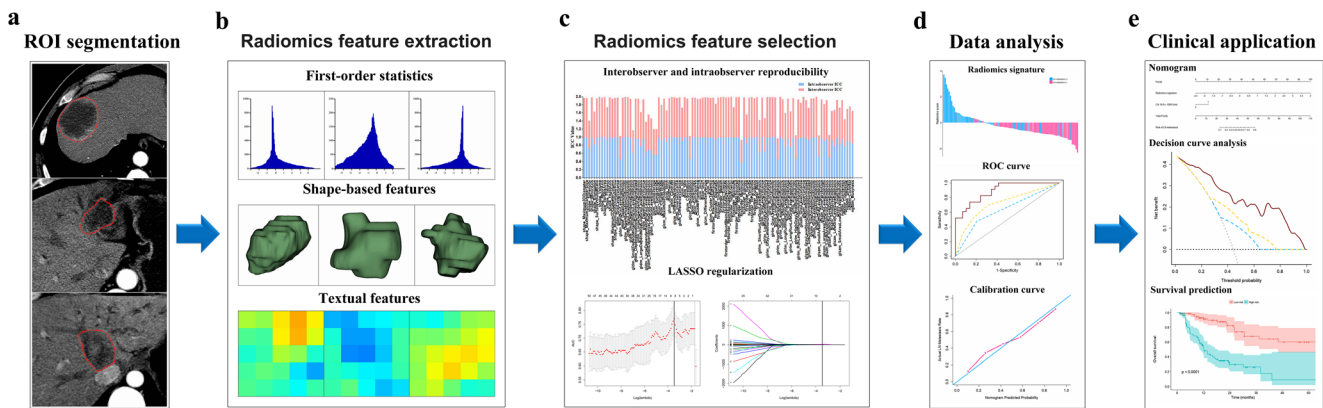


Fig. 1 Workflow of necessary steps in this study. **a** Tumors were contoured manually on all axial arterial phase CT slices. **b** Radiomics features were extracted from within the defined tumor contours to quantify tumor intensity, shape, and texture. **c** Two feature selection steps were applied to all extracted features. **d** A radiomics signature was constructed using a linear combination of selected features. The performance of prediction models was determined using AUC value

type and peripheral type according to the presence or absence of tumor invasion of the hepatic hilum; (c) vascular invasion, defined as vessel occlusion, stenosis, or contour deformity associated with tumor invasion; and (d) positive LN metastasis, defined as a short-axis diameter over 10 mm, central necrosis, or hyperattenuating compared with liver parenchyma in the portal phase [6, 19, 21]. Any discrepant interpretation was resolved through consultation.

The radiomics workflow is depicted in Fig. 1. Arterial phase CT images at 1.5 mm thickness were retrieved for image feature extraction. Tumor regions of interest (ROIs) were manually segmented by two independent observers (see below) along the primary tumor contour on each transverse slice using an open-source software 3D Slicer (version 4.9.0; www.slicer.org). After installation of a dependent radiomics module, a total of 105 radiomics features, quantifying phenotypic differences based on shape ($n = 13$), first-order ($n = 18$), and texture ($n = 74$) features, were extracted from the three-dimensional ROIs [22]. Details of feature algorithms are described in the [Supplementary methods](#).

Radiomics feature selection and signature construction

A two-step procedure was devised for dimensionality reduction. First, we randomly chose 20 patients for ROI segmentation and feature extraction. To determine interobserver reproducibility, ROI segmentations were performed in a blinded fashion by one radiologist (reader 1, F.P.Z.) and one hepatobiliary surgeon (reader 2, G.W.J. with 5 years of experience in hepatobiliary surgery and imaging); both were aware of the diagnosis of IHC but were blinded to the clinicopathologic details. To evaluate intraobserver reproducibility, reader 1 repeated the same procedure 1 month later. The remaining

and calibration curve. **e** A nomogram that incorporates radiomics signature and independent risk factors was built to provide a more understandable outcome measure for individualized evaluation, followed by decision curve analysis and survival prediction. ROI, region of interest; LASSO, least absolute shrinkage and selection operator; ROC, receiver operating characteristic

image segmentations were then completed by reader 1. The intraclass correlation coefficient (ICC) was used to assess reproducibility of feature extraction. Only features with both intraobserver and interobserver ICC values greater than 0.90 were initially selected. Second, the least absolute shrinkage and selection operator (LASSO) logistic regression algorithm [23], with penalty parameter tuning conducted by 10-fold cross-validation, was used to select robust and nonredundant features from the primary cohort. A radiomics signature was created by a linear combination of selected features weighted by their respective coefficients, and the corresponding radiomics score was calculated for each patient.

Development, performance, and validation of a radiomics nomogram

A radiomics model that incorporated the radiomics signature and independent various risk factors for predicting LN metastasis was built based on multivariate logistic regression analysis in the primary cohort. We checked the variables included in the regression equations for multicollinearity using variance inflation factor (VIF) [24]. A radiomics nomogram was then constructed using the selected covariates to provide a visual tool for clinical use. In addition, a clinical model was developed based on multivariate logistic regression analysis of candidate predictors with the exception of radiomics signature.

We determined the area under the curve (AUC) of the receiver operating characteristic curve (ROC) to assess the discrimination performance of established models [25]. Differences in AUC estimates between various models were compared using the DeLong algorithm [26]. Calibration curves were plotted via bootstrapping with 1000 resamples to evaluate the predictive accuracy of the radiomics nomogram, accompanied by the Hosmer–Lemeshow test. Internal

validation of established models was performed using an independent dataset.

All patients were divided into high-risk or low-risk metastasis groups according to the radiomics nomogram. The threshold for dichotomization was selected based on the maximized Youden index [27].

Clinical utility of the radiomics nomogram

To estimate the clinical utility of established models, decision curve analysis (DCA) was performed by quantifying the net benefits at different threshold probabilities in the validation dataset [28].

Statistical analysis

Numerical variables were compared by means of the *t* test or Mann–Whitney *U* test, and categorical variables were compared using the χ^2 test or Fisher's exact test, when appropriate. Overall survival (OS) was computed as the interval between the date of surgery and the date of death or last follow-up. Recurrence-free survival (RFS) was defined as the interval between surgery and radiographic detection of recurrence or last follow-up. Survival curves were depicted using the Kaplan–Meier method and compared using the log-rank test. Univariate and multivariate Cox regression analyses were performed to determine predictors of OS and RFS. All variables with *p* value < 0.05 in univariate analysis were selected for multivariate analysis. Statistical analysis was done with R (version 3.4.4) with R packages listed in the [Supplementary methods](#). A two-sided *p* value < 0.05 was considered significant.

Results

Patient characteristics

Demographic and baseline characteristics of all patients are summarized in Table 1 and Supplementary Table S1. The rates of LN metastasis were 43.7 and 44.2% in the primary and validation cohorts, respectively, while no significant difference was found between the two cohorts (*p* = 0.949). In total, 35 patients (51.5%, 35/68) with nodal metastasis were understaged and 20 patients (23.0%, 20/87) without nodal metastasis were overstaged based on CT-reported LN status.

Feature selection and radiomics signature construction

Of the 105 radiomics features, 67 most stable features (both intraobserver and interobserver ICC values greater than 0.90) were selected for subsequent analysis. Eight LN-status-related features with nonzero coefficients in the LASSO logistic regression model were screened based on the primary cohort (Fig. 2). A radiomics signature was then constructed using the calculation formula presented in the [Supplementary material](#). Distributions of the radiomics score and LN status for each patient in the primary and validation cohorts are shown in Supplementary Fig. S2.

Diagnostic validation of radiomics signature

A significant difference in radiomics score was initially evidenced between patients with and those without LN

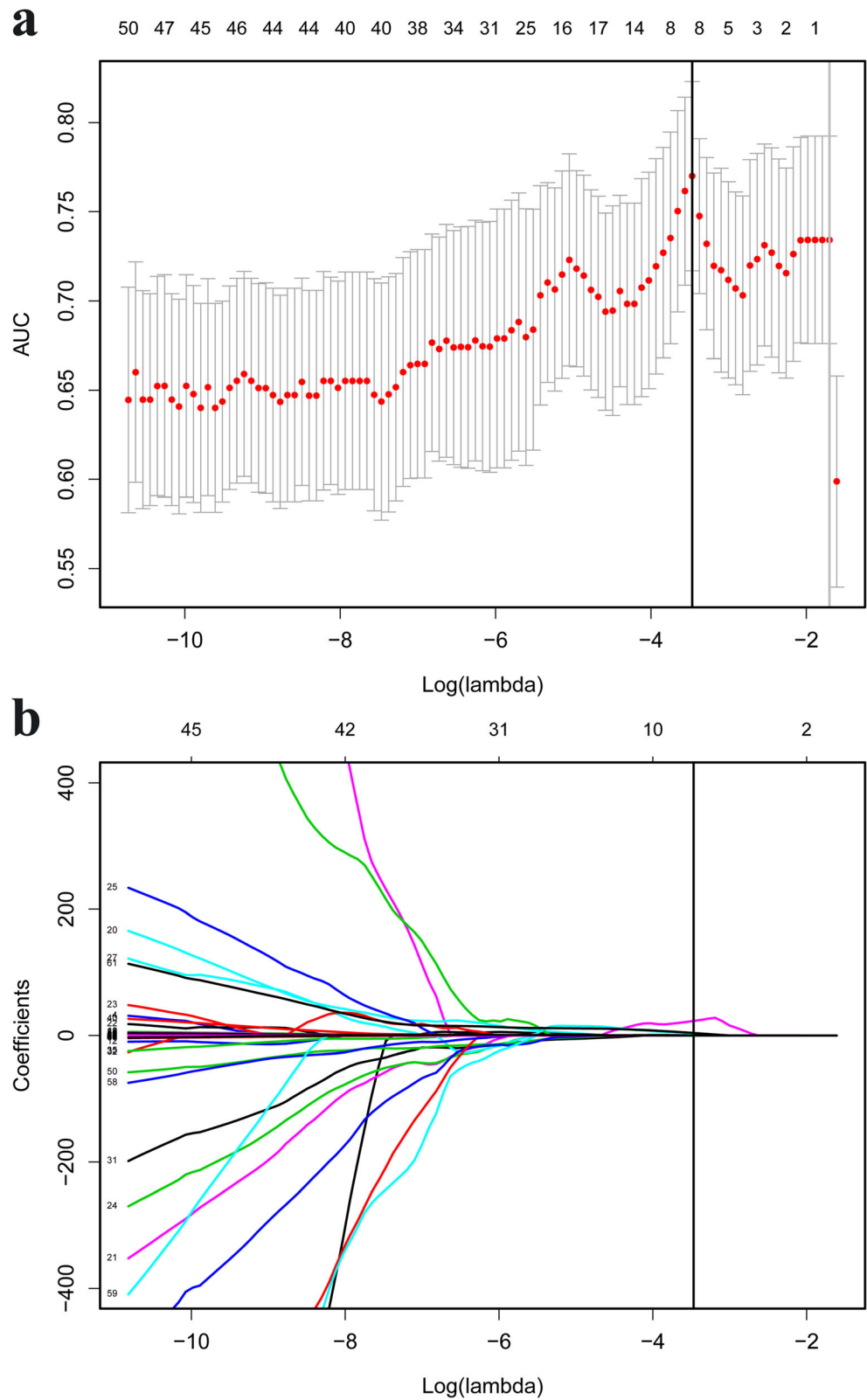
Table 1 Clinical characteristics of patients in the primary and validation cohorts

Characteristics	Primary cohort (<i>n</i> = 103)			Validation cohort (<i>n</i> = 52)		
	LN metastasis (–)	LN metastasis (+)	<i>p</i> value	LN metastasis (–)	LN metastasis (+)	<i>p</i> value
Age, mean ± SD, years	59.9 ± 10.9	60.5 ± 8.4	0.646	60.1 ± 10.0	61.0 ± 8.7	0.644
Gender			0.755			0.829
Male	34 (58.6)	25 (55.6)		16 (55.2)	12 (52.2)	
Female	24 (41.4)	20 (44.4)		13 (44.8)	11 (47.8)	
Tumor location			0.630			0.463
Peripheral	36 (62.1)	30 (66.7)		16 (55.2)	15 (65.2)	
Perihilar	22 (37.9)	15 (33.3)		13 (44.8)	8 (34.8)	
Hepatitis B virus infection	9 (15.5)	8 (17.8)	0.759	5 (17.2)	7 (30.4)	0.262
CA 19-9 level ≥ 1000 U/ml	11 (19.0)	21 (46.7)	0.003	5 (17.2)	12 (52.2)	0.008
CT-reported vascular invasion	23 (39.7)	24 (53.3)	0.167	14 (48.3)	13 (56.5)	0.555
CT-reported tumor size > 5 cm	19 (32.8)	22 (48.9)	0.097	11 (37.9)	12 (57.2)	0.304
CT-reported LN status			0.009			0.038
LN negative	44 (75.9)	23 (51.1)		23 (79.3)	12 (52.2)	
LN positive	14 (24.1)	22 (48.9)		6 (20.7)	11 (47.8)	
Radiomics score, median (interquartile range)	–0.762 (–1.004 to –0.370)	0.186 (–0.476 to 0.721)	< 0.001	–0.876 (–1.099 to –0.334)	0.133 (–0.176 to 0.386)	< 0.001

Data are the number of patients with percentage in parentheses unless otherwise indicated

LN, lymph node; SD, standard deviation; CA 19-9, carbohydrate antigen 19-9; CT, computed tomography

Fig. 2 Radiomics feature selection using a parametric method, the LASSO logistic regression. **a** Selection of tuning parameter (λ) in the LASSO model used 10-fold cross-validation via minimum criteria. The AUC curve was plotted versus $\log(\lambda)$. Vertical lines were drawn at the optimal values by using the minimum criteria and the 1 standard error of the minimum criteria (the 1-SE criteria). The optimal λ value of 0.0311 with $\log(\lambda) = -3.4694$ was chosen. **b** LASSO coefficient profiles of 67 selected features. A vertical line was plotted at the value selected using 10-fold cross-validation, where optimal λ resulted in eight features with nonzero coefficients. LASSO, least absolute shrinkage and selection operator



metastasis in the primary cohort ($p < 0.001$), and then confirmed in the validation cohort ($p < 0.001$). The radiomics signature yielded an AUC of 0.8228 (95%

CI, 0.7391–0.9065) in the primary cohort and 0.8711 (95% CI, 0.7746–0.9676) in the validation cohort, indicating favorable predictive efficacy.

Table 2 Multivariate logistic regression analysis for LN metastasis in the primary cohort

Variables	Radiomics model		Clinical model *	
	Odds ratio (95% CI)	<i>p</i> value	Odds ratio (95% CI)	<i>p</i> value
CA 19-9 \geq 1000 U/ml	4.107 (1.433–11.771)	0.009	3.372 (1.367–8.319)	0.008
CT-reported LN status	1.169 (0.401–3.404)	0.775	2.668 (1.116–6.379)	0.027
Radiomics signature	7.309 (2.821–18.942)	<0.001	NA	NA

CI, confidence interval; CA 19-9, carbohydrate antigen 19-9; CT, computed tomography; LN, lymph node; NA, not available

*A clinical model was built based on independent predictors of nodal metastasis without the addition of radiomics signature

Development, performance, and validation of prediction models

Results of multivariate regression analysis are shown in Table 2. The VIFs of three potential predictors ranged from 1.05 to 1.09, indicating that there was no multicollinearity. A radiomics model that incorporated two independent predictors (radiomics signature and CA 19-9 \geq 1000 U/ml) was constructed and presented as a nomogram (Fig. 3a). On the other hand, a clinical prediction model was developed based on two independent predictors (CT-reported LN status and CA 19-9 \geq 1000 U/ml) of LN metastasis without the addition of radiomics signature.

ROC analyses comparing the discriminatory ability of the radiomics nomogram to those of the clinical model and CT-reported LN status alone are given in Fig. 3b, c. In the primary cohort, the radiomics nomogram yielded the highest discrimination between LN positive and negative, with an AUC of 0.8462 (95% CI, 0.7676–0.9248); the observed AUC value was significantly higher than that of the clinical model (AUC 0.7136; 95% CI, 0.6174–0.8098; $p = 0.046$) and CT-reported LN status alone (AUC 0.6238; 95% CI, 0.5313–0.7162; $p < 0.001$). In the validation cohort, the radiomics model also yielded the greatest AUC of 0.8921 (95% CI, 0.8096–0.9745) that supported the improved predictive efficacy as compared with either the clinical model (AUC 0.7219; 95% CI, 0.5882–0.8555; $p = 0.012$) or CT-reported LN status alone (AUC 0.6357; 95% CI, 0.5071–0.7642; $p = 0.001$). The calibration curve and the Hosmer–Lemeshow test statistic ($p = 0.6398$) demonstrated favorable calibration of the nomogram in the primary cohort (Fig. 3d). Good calibration was further confirmed in the validation cohort (Fig. 3e), and the Hosmer–Lemeshow test yielded a p value of 0.8197, suggesting a perfect fit of the nomogram. Within the CT-reported LN-negative subgroup, the AUC for the radiomics nomogram was 0.9224 (95% CI, 0.8661–0.9787), significantly higher than that for the clinical model (AUC 0.6832; 95% CI, 0.5905–0.7758; $p < 0.001$).

After obtaining risk scores from the radiomics model and choosing the optimal cutoff value of -0.535 (corresponding

total 41 points in the nomogram) at the point of the maximum Youden index from the entire cohort, all patients were classified into low-risk or high-risk group. Significant discrimination of LN metastasis between high-risk and low-risk groups was observed in the entire cohort and the CT-reported LN-negative subgroup (both $p < 0.001$) (Supplementary Table S2). According to this risk classifier, the radiomics model achieved a sensitivity of 86.8% and a specificity of 73.6% for predicting LN status in the entire cohort, while positive predictive value (PPV) and negative predictive value (NPV) were 72.0 and 87.7%, respectively. Moreover, overall accuracy of this risk classifier in the CT-reported LN-negative subgroup was 87.3%, with a sensitivity of 94.3%, a specificity of 83.6%, PPV of 75.0%, and NPV of 96.6% (Fig. 4).

Clinical use

DCA for the radiomics nomogram, clinical model, and CT-reported LN status is presented in Fig. 5. The radiomics-based nomogram provides a better net benefit than “treat-all” or “treat-none” schemes and other two models for all threshold probabilities.

Preoperative predictors of survival

Median OS and RFS for the entire cohort were 30.3 and 18.1 months after a median follow-up of 14.0 (range 1.1–97.9) months. Kaplan–Meier curves demonstrated that the radiomics nomogram was significantly associated with OS and RFS in the overall cohort (both $p < 0.001$) (Fig. 6). Although median OS was not available, median RFS was 51.0 months in the low-risk group, with estimated 5-year OS rate of 59.7% and RFS rate of 44.1%. However, median OS and RFS in the high-risk group were only 12.2 and 8.8 months, with estimated 5-year OS rate of 8.7% and RFS rate of 6.1%. Univariate and multivariate Cox regression analyses confirmed that high-risk LN metastasis was an independent preoperative factor for unfavorable OS (HR 3.65; 95% CI, 1.95–6.80;

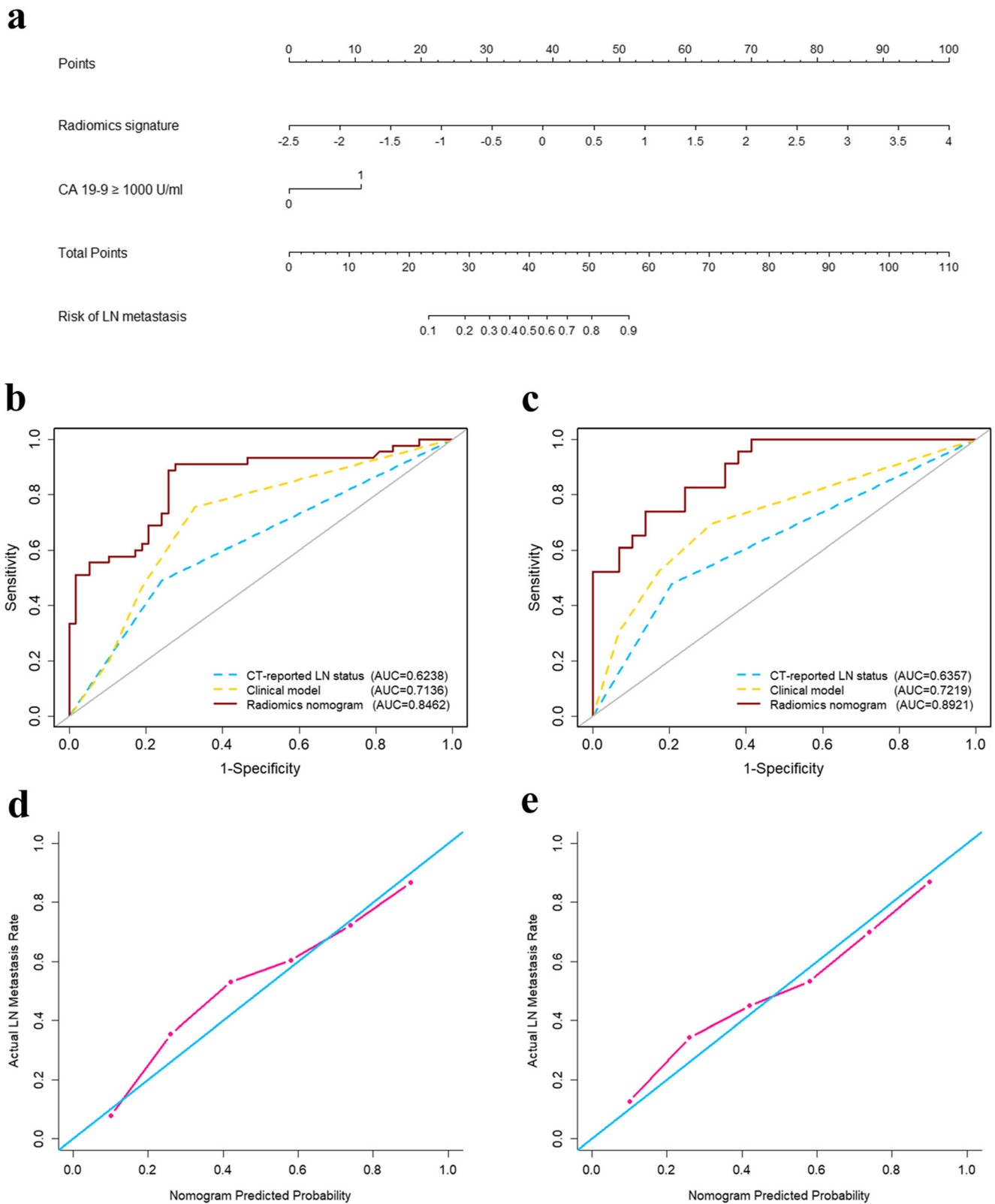


Fig. 3 Radiomics nomogram developed with ROC and calibration curves. A radiomics nomogram was established based on the primary cohort, with radiomics signature and preoperative CA 19-9 level incorporated (a). Comparison of ROC curves between radiomics nomogram, clinical model, and CT-reported LN status

alone for prediction of LN metastasis in the primary (b) and validation (c) cohorts. Calibration curves of radiomics nomogram in the primary (d) and validation (e) cohorts. ROC, receiver operating characteristic; LN, lymph node

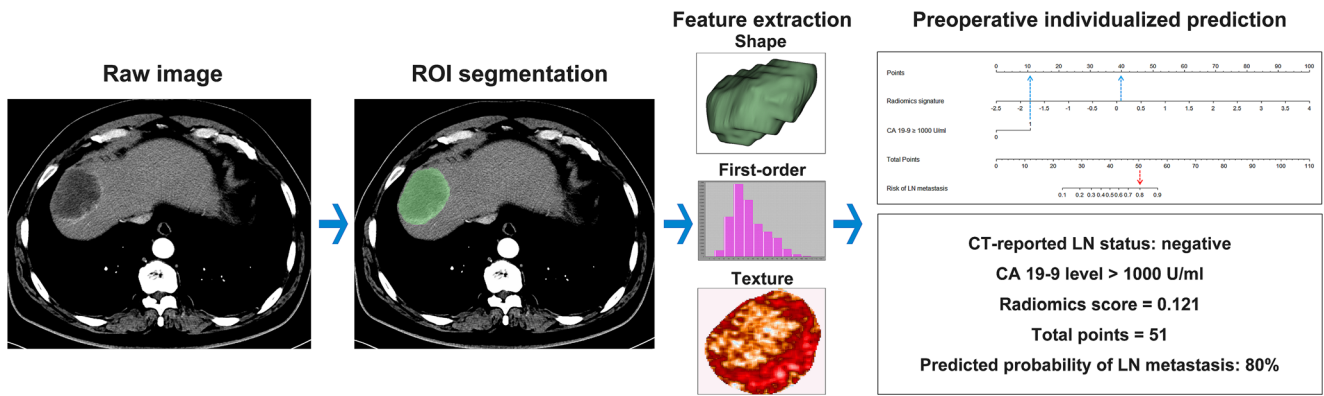


Fig. 4 An example of how to use the radiomics nomogram to predict LN metastasis in a 61-year-old male patient with radiologically negative LN. ROI, region of interest; LN, lymph node

$p < 0.001$) and RFS (HR 2.77; 95% CI, 1.58–4.84; $p < 0.001$), as was preoperative CA 19-9 level (Table 3).

With the addition of pathologic results, actual LN status and radiomics nomogram were evaluated separately in multivariate Cox regression analyses because of collinearity between the two variables; our radiomics nomogram predicted survival outcomes in a manner similar to actual LN status (Supplementary Tables S3 and S4).

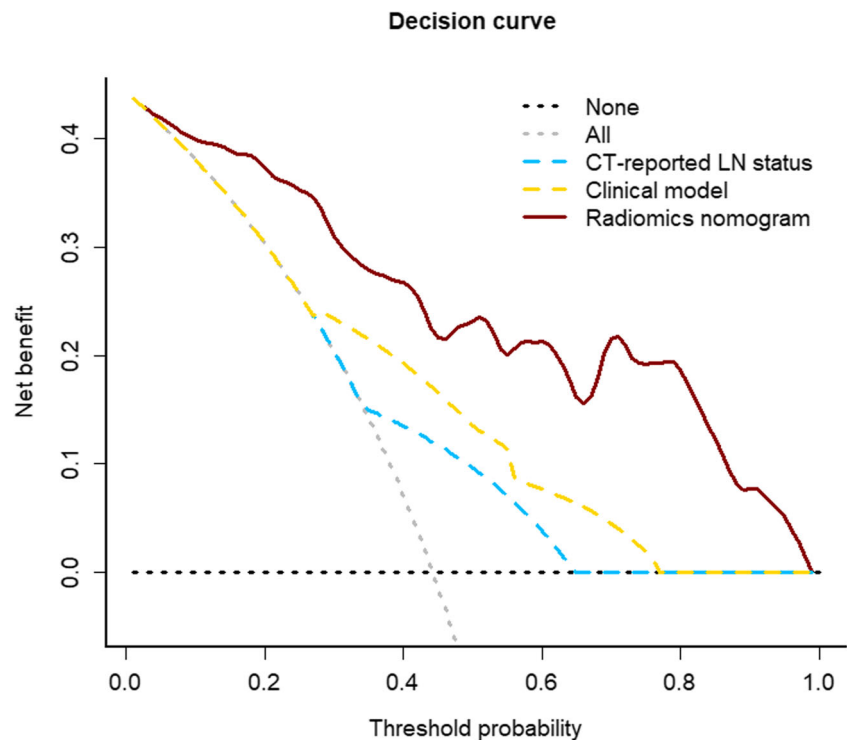
Discussion

In this study, we investigated the utility of a radiomics-based model to predict LN metastasis in patients with IHCs before surgery. A radiomics signature consisted of

eight robust features and successfully stratified patients according to their statistical risk of LN metastasis. An easy-to-use radiomics nomogram that incorporates radiomics signature and CA 19-9 level achieved significantly better performance than clinical prediction model and nodal morphology. Moreover, the predicted LN metastasis risk according to our radiomics nomogram emerged as an independent preoperative predictor of survival outcomes following curative-intent surgery, thereby providing important information for medical decision support.

Discrimination of malignant from benign nodes on cross-sectional imaging with traditional practice of visual interpretation remains challenging. In this study, enhanced CT for nodal staging was inaccurate in up to 35% of patients and,

Fig. 5 Decision curve analysis for each model in the validation dataset. The y-axis measures the net benefit. The red line represents the radiomics nomogram. The yellow line represents the clinical prediction model. The blue line represents CT-reported LN status alone. The gray dotted line represents the assumption that all patients had LN metastasis. The black dotted line represents the assumption that no patients had LN metastasis. LN, lymph node



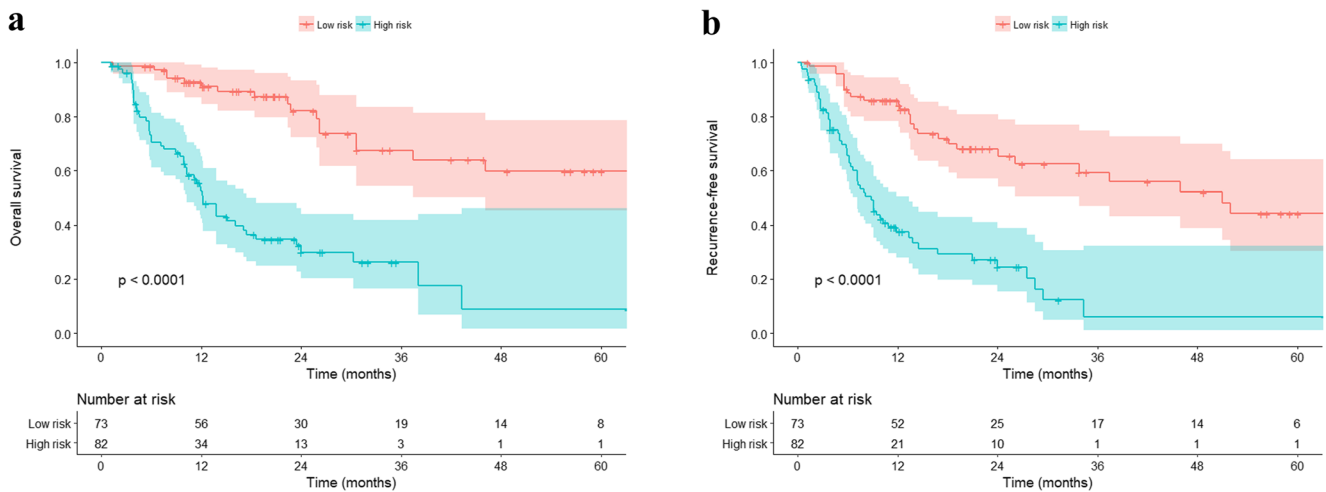


Fig. 6 Survival of patients stratified by the risk classification according to the radiomics nomogram in the entire cohort ($n = 155$). Overall survival (a) and recurrence-free survival (b) were significantly worse in patients at

high risk of lymph node metastasis compared with those at low risk after curative-intent resection. Shaded areas represent 95% confidence intervals

therefore, should not be considered as a valid alternative to perform lymphadenectomy. Although positron emission tomography scans have beneficial effects for assessment of occult nodal metastasis, the reported sensitivity is merely 13–38% [11]. These data suggest that current imaging modalities based on morphologic criteria or metabolic activity fail to accurately predict nodal status. This may be attributed to small nodal metastasis and nonspecific inflammatory hyperplasia [29, 30]. Alternatively, inter- and intratumor heterogeneity indicates a high propensity for metastatic disease [31]. However, information derived from a standard workup with conventional imaging refers to simple semantic traits, which have limited the potential for precision medicine. Conversely, radiomics approaches provide important complementary data on the imaging phenotype that may encompass a wealth of information. Among the eight selected radiomics features, five texture features describe the patterns or spatial distribution of voxel intensities within the ROI and, therefore, capture tumor

heterogeneity; a greater value is indicative of more heterogeneity and tumor metastasis. For predicting LN metastasis, the radiomics signature derived from arterial phase images in this study achieved AUC over 0.80 in IHCs, better than that derived from portal venous phase images in BTCs [18]. The radiomics-based predictive tool serves as a better surrogate of LN metastasis than do nodal morphology. Given that LN positivity is comparable between the primary and validation sets, our data suggest that the proposed radiomics nomogram facilitates individualized prediction of LN metastasis and may have broad clinical applicability.

In a study by Yoh et al [32], a clinical risk score, consisting of CA 19-9 level, hilar invasion, and CT-reported LN status, showed good discrimination for LN metastasis in IHCs, with an AUC of 0.874; however, no validation was performed. As an alternative, a clinical prediction model was also developed without radiomics signature in this study. The clinical model incorporates preoperative CA 19-9 level and CT-reported LN

Table 3 Uni- and multivariate Cox regression analyses of preoperative predictors of overall and recurrence-free survival

Variables	Overall survival				Recurrence-free survival			
	Univariate		Multivariate		Univariate		Multivariate	
	HR (95% CI)	<i>p</i> value	HR (95% CI)	<i>p</i> value	HR (95% CI)	<i>p</i> value	HR (95% CI)	<i>p</i> value
Age (≥ 60 vs < 60 years)	1.50 (0.91–2.45)	0.110			1.01 (0.65–1.56)	0.950		
Sex (male vs female)	1.36 (0.84–2.22)	0.211			1.12 (0.73–1.73)	0.600		
Tumor location (hilar vs peripheral)	1.51 (0.94–2.43)	0.088			1.64 (1.07–2.51)	0.024	0.87 (0.52–1.45)	0.596
Hepatitis B virus infection (yes vs no)	0.85 (0.43–1.58)	0.601			1.04 (0.60–1.81)	0.878		
CA 19-9 level (≥ 1000 vs < 1000 U/ml)	3.88 (2.38–6.32)	< 0.001	1.95 (1.11–3.43)	0.020	3.73 (2.37–5.86)	< 0.001	2.11 (1.16–3.84)	0.015
CT-reported tumor size (> 5 vs ≤ 5 cm)	1.23 (0.77–1.99)	0.388			0.90 (0.58–1.41)	0.647		
CT-reported vascular invasion (yes vs no)	0.99 (0.62–1.59)	0.964			1.19 (0.78–1.82)	0.424		
CT-reported LN status (positive vs negative)	1.76 (1.10–2.81)	0.019	1.32 (0.80–2.17)	0.274	1.73 (1.13–2.65)	0.012	1.40 (0.89–2.20)	0.145
Radiomics nomogram (high risk vs low risk)	5.05 (2.90–8.81)	< 0.001	3.65 (1.95–6.83)	< 0.001	3.92 (2.44–6.32)	< 0.001	2.77 (1.58–4.84)	< 0.001

HR, hazard ratio; CI, confidence interval; CA 19-9, carbohydrate antigen 19-9; CT, computed tomography; LN, lymph node

status, showing better predictive efficacy than CT-reported LN status alone, but significantly inferior to the radiomics nomogram. Note that 34.3% of patients (35/102) harbored radiologically occult nodal metastasis in this study. For patients with macroscopically normal nodes on CT images, our score-based risk classifier had 87.3% accuracy for detection of nodal involvement and low-risk patients showed an actual metastasis rate of only 3.4%.

Promisingly, our radiomics nomogram showed highly significant differences in survival outcomes between IHCs predicted to have high-risk and low-risk LN metastases. Patients at high risk of LN metastasis according to our radiomics nomogram had a 5-fold increased risk of death and 4-fold increased risk of disease recurrence compared with low-risk patients. Given that long-term outcomes in the high-risk group were not satisfactory even after curative-intent resection, neoadjuvant therapy may be indicated for high-risk subsets to evaluate tumor biology and define patients most likely to benefit from surgical intervention. Accordingly, our radiomics-based model may alter indications for surgery, thus being applied within clinical decision support systems for personalized treatment.

The current study had several limitations. First, the model is established based on single-center data and prospective multicenter studies are needed to further validate our results. Second, the imaging–surgical–pathologic correlation of LN metastasis was not assessed on a station-by-station basis. False-negative diagnosis of nodal metastasis cannot be ruled out due to inadequate LN sampling. Additionally, tumor location was not associated with LN metastasis in this study; however, some investigators have reported that nodal metastasis is more frequent in IHCs of large-duct type than in those of small-duct type [2, 33, 34]. This discrepancy may be explained considering the interreader variance in imaging interpretations.

In conclusion, we proposed and internally validated a radiomics nomogram to predict LN metastasis in IHC patients before surgery, especially in the CT-reported LN-negative subgroup. This easy-to-use nomogram predicts nodal metastasis with high accuracy and risk stratifies survival outcomes; thus, our radiomics model may facilitate clinical decision-making and define patient subsets benefiting most from surgery.

Funding This study was supported by the Natural Science Foundation of China (81530048, 81470901, 81670570) and the Key Research and Development Program of Jiangsu Province (BE2016789).

Compliance with ethical standards

Guarantor The scientific guarantor of this publication is Xue-Hao Wang.

Conflict of interest The authors declare that they have no conflict of interest.

Statistics and biometry No complex statistical methods were necessary for this paper.

Informed consent Written informed consent was waived by the Institutional Review Board.

Ethical approval Institutional Review Board approval was obtained.

Methodology

- Retrospective
- Diagnostic or prognostic study
- Performed at one institution

References

1. Rizvi S, Khan SA, Hallemeier CL, Kelley RK, Gores GJ (2018) Cholangiocarcinoma—evolving concepts and therapeutic strategies. *Nat Rev Clin Oncol* 15:95–111
2. Joo I, Lee JM, Yoon JH (2018) Imaging diagnosis of intrahepatic and perihilar cholangiocarcinoma: recent advances and challenges. *Radiology* 288:7–13
3. Khan SA, Davidson BR, Goldin RD et al (2014) Guidelines for the diagnosis and management of intrahepatic cholangiocarcinoma. *J Hepatol* 60:1268–1289
4. Zhang XF, Beal EW, Bagante F et al (2018) Early versus late recurrence of intrahepatic cholangiocarcinoma after resection with curative intent. *Br J Surg* 105:848–856
5. Zhang XF, Chakedis J, Bagante F et al (2018) Trends in use of lymphadenectomy in surgery with curative intent for intrahepatic cholangiocarcinoma. *Br J Surg* 105:857–866
6. Adachi T, Eguchi S, Beppu T et al (2015) Prognostic impact of preoperative lymph node enlargement in intrahepatic cholangiocarcinoma: a multi-institutional study by the Kyushu Study Group of Liver Surgery. *Ann Surg Oncol* 22:2269–2278
7. de Jong MC, Nathan H, Sotiropoulos GC et al (2011) Intrahepatic cholangiocarcinoma: an international multi-institutional analysis of prognostic factors and lymph node assessment. *J Clin Oncol* 29:3140–3145
8. Morine Y, Shimada M (2015) The value of systematic lymph node dissection for intrahepatic cholangiocarcinoma from the viewpoint of liver lymphatics. *J Gastroenterol* 50:913–927
9. Benson AB 3rd, D’Angelica MI, Abrams TA et al (2014) Hepatobiliary cancers, version 2.2014. *J Natl Compr Cancer Netw* 12:1152–1182
10. Razumilava N, Gores GJ (2014) Cholangiocarcinoma. *Lancet* 383:2168–2179
11. Blechacz B, Komuta M, Roskams T, Gores GJ (2011) Clinical diagnosis and staging of cholangiocarcinoma. *Nat Rev Gastroenterol Hepatol* 8:512–522
12. Lambin P, Leijenaar RTH, Deist TM et al (2017) Radiomics: the bridge between medical imaging and personalized medicine. *Nat Rev Clin Oncol* 14:749–762
13. Limkin EJ, Sun R, Derclé L et al (2017) Promises and challenges for the implementation of computational medical imaging (radiomics) in oncology. *Ann Oncol* 28:1191–1206
14. Aerts HJ (2016) The potential of radiomic-based phenotyping in precision medicine: a review. *JAMA Oncol* 2:1636–1642
15. Huang YQ, Liang CH, He L et al (2016) Development and validation of a radiomics nomogram for preoperative prediction of lymph node metastasis in colorectal cancer. *J Clin Oncol* 34:2157–2164
16. Wu S, Zheng J, Li Y et al (2017) A radiomics nomogram for the preoperative prediction of lymph node metastasis in bladder cancer. *Clin Cancer Res* 23:6904–6911

17. Gu Y, She Y, Xie D et al (2018) A texture analysis-based prediction model for lymph node metastasis in stage IA lung adenocarcinoma. *Ann Thorac Surg* 106:214–220
18. Ji GW, Zhang YD, Zhang H et al (2019) Biliary tract cancer at CT: a radiomics-based model to predict lymph node metastasis and survival outcomes. *Radiology* 290:90–98
19. Kim SA, Lee JM, Lee KB et al (2011) Intrahepatic mass-forming cholangiocarcinomas: enhancement patterns at multiphasic CT, with special emphasis on arterial enhancement pattern—correlation with clinicopathologic findings. *Radiology* 260:148–157
20. Yamamoto Y, Türkoğlu MA, Aramaki T et al (2016) Vascularity of intrahepatic cholangiocarcinoma on computed tomography is predictive of lymph node metastasis. *Ann Surg Oncol* 23:485–493
21. Lee HY, Kim SH, Lee JM et al (2006) Preoperative assessment of resectability of hepatic hilar cholangiocarcinoma: combined CT and cholangiography with revised criteria. *Radiology* 239:113–121
22. van Griethuysen JJM, Fedorov A, Parmar C et al (2017) Computational radiomics system to decode the radiographic phenotype. *Cancer Res* 77:e104–e107
23. Tibshirani R (1996) Regression shrinkage and selection via the lasso. *J R Stat Soc Ser B Stat Methodol* 58:267–288
24. Kutner MH, Nachtsheim C, Neter J (2004) *Applied linear regression models*. McGraw-Hill/Irwin
25. Hanley JA, McNeil BJ (1982) The meaning and use of the area under a receiver operating characteristic (ROC) curve. *Radiology* 143:29–36
26. DeLong ER, DeLong DM, Clarke-Pearson DL (1988) Comparing the areas under two or more correlated receiver operating characteristic curves: a nonparametric approach. *Biometrics* 44:837–845
27. Youden WJ (1950) Index for rating diagnostic tests. *Cancer* 3:32–35
28. Fitzgerald M, Saville BR, Lewis RJ (2015) Decision curve analysis. *JAMA* 313:409–410
29. Ruys AT, Kate FJ, Busch OR, Engelbrecht MR, Gouma DJ, van Gulik TM (2011) Metastatic lymph nodes in hilar cholangiocarcinoma: does size matter? *HPB (Oxford)* 13:881–886
30. Thoeny HC, Froehlich JM, Triantafyllou M et al (2014) Metastases in normal-sized pelvic lymph nodes: detection with diffusion-weighted MR imaging. *Radiology* 273:125–135
31. Bedard PL, Hansen AR, Ratain MJ, Siu LL (2013) Tumour heterogeneity in the clinic. *Nature* 501:355–364
32. Yoh T, Hatano E, Seo S et al (2018) Preoperative criterion identifying a low-risk group for lymph node metastasis in intrahepatic cholangiocarcinoma. *J Hepatobiliary Pancreat Sci* 25:299–307
33. Asayama Y, Yoshimitsu K, Irie H et al (2006) Delayed-phase dynamic CT enhancement as a prognostic factor for mass-forming intrahepatic cholangiocarcinoma. *Radiology* 238:150–155
34. Rhee H, Kim MJ, Park YN, An C (2018) A proposal of imaging classification of intrahepatic mass-forming cholangiocarcinoma into ductal and parenchymal types: clinicopathologic significance. *Eur Radiol*. <https://doi.org/10.1007/s00330-018-5898-9>

Publisher's note Springer Nature remains neutral with regard to jurisdictional claims in published maps and institutional affiliations.